Mine Detection using SF-GPR: A Signal Processing Approach for Resolution Enhancement and Clutter Reduction

Brian Karlsen[a], Kaj B. Jakobsen[b], Jan Larsen[c], and Helge B.D. Sørensen[a]

[a]Ørsted•DTU - Electronics and Signal Processing,
The Technical University of Denmark,
Building 451, DK-2800 Kongens Lyngby, Denmark.

[b]Ørsted•DTU - Electromagnetic Systems,
The Technical University of Denmark,
Ørsteds Plads, Building 348, DK-2800 Kongens Lyngby, Denmark.

[c]Informatics and Mathematical Modelling - Section for Digital Signal Processing
Technical University of Denmark,
Richard Petersens Plads, Building 321, DK-2800 Kongens Lyngby, Denmark.

ABSTRACT

Proper clutter reduction is essential for Ground Penetrating Radar data since low signal-to-clutter ratio prevent correct detection of mine objects. A signal processing approach for resolution enhancement and clutter reduction used on Stepped-Frequency Ground Penetrating Radar (SF-GPR) data is presented, and the effects of combining clutter reduction with resolution enhancement are examined using simulated SF-GPR data examples. The resolution enhancement method is based on methods from optical signal processing and is largely carried out in the frequency domain to reduce the computational burden. The clutter reduction method is based on basis function decomposition of the SF-GPR time-series from which the clutter and the signal are separated.

Keywords: Anti-personal mine detection, stepped-frequency GPR, resolution enhancement, optical signal processing, clutter reduction, PCA subspace decomposition.

1. INTRODUCTION

Mines and other explosive ordnances buried below the ground surface are an increasing threat to civilians and military forces in many war-torn and developing countries. The overall objective of the approaches presented in this paper is to identify small mine-like metallic and non-metallic objects buried in the ground using a Stepped-Frequency Ground Penetrating Radar (SF-GPR), which is one of the most promising mine detectors.

Mines, especially anti-personal mines, are in general buried close to the surface of the ground. Small mines buried close to the ground surface are difficult to detect using a GPR due to the fact that the GPR signals are hampered by a low signal-to-clutter ratio and a low signal-to-noise ratio[2].

To increase the detection probability of mines, the signal-to-noise ratio must be improved. When using a monostatic SF-GPR, the energy reflected from the objects buried in the ground are spatially smeared. The smeared energy can be focus using various imaging techniques and thereby increasing the signal-to-noise ratio. Several imaging methods have been discussed in the literature. The majority of the methods are derived from the inverse time migration method[3] and the Stolt $\omega - k$ migration method[10], which are widely used examples of time-domain and frequency-domain approaches, respectively. In this paper we suggest an approach inspired by optical signal processing, which mainly is carried out in the frequency domain.

The clutter that effects a SF-GPR can be defined as those signals that are unrelated to the target scattering characteristics but occupy the same frequency band as the targets. Clutter can be caused by multiple reflections,

Author information on *BK*: brk@oersted.dtu.dk, www.oersted.dtu.dk; *KBJ*: kbj@oersted.dtu.dk, www.oersted.dtu.dk; *JL*: jl@imm.dtu.dk, www.imm.dtu.dk/ jl; *HBDS*: hbs@oersted.dtu.dk, www.oersted.dtu.dk

e.g., in the antenna, between the antenna and the ground surface, and the none mine targets buried in the ground. The clutter hamper the improvements that can be obtained using imaging processing and thereby prevent an increase in the signal-to-noise ratio. In general, clutter is more significant at close ranges and reduces when the range gets larger, primarily because of the longer distances between the reflection surfaces and the losses in the ground[2]. This is the reason why clutter is most severe for near the surface placed landmines, which calls for clutter reduction. Several clutter reduction techniques have been deployed on GPR signals[2], but none do provide sufficient suppression due to the stochastic nature of the ground surface. A classical method is the well known mean-subtraction method[2], where the average value of the ensemble of one- or two-dimensional scan area is subtracted from each of the considered one-dimensional scans. Recently[7] we suggested a subspace decomposing technique based on subspace decomposing using Principal Component Analysis (PCA) in which highly correlated spatial clutter is removed. PCA has previously been applied to GPR data both for the detection of mines[13] and for clutter reduction[4]. Our approach taken here is different and inspired by explorative analysis of functional neuroimages[5].

This paper compares simple mean-subtraction versus PCA based clutter reduction in combination with resolution enhancement. The results are based on simulated SF-GPR data in the S-band (2.65 GHz - 3.95 GHz). In typical practical settings this bandwidth is realistic and has been used in previous work[7].

In Section 2 the clutter reduction approach is discussed. The resolution enhancement approach is presented in Section 3. In Section 4 the deployed SF-GPR system and simulated SF-GPR signals are described. Finally, examples and results of the clutter reduction and the resolution enhancement approaches are presented in Section 5.

2. CLUTTER REDUCTION BASED ON SUBSPACE DECOMPOSING

Due to the stochastic nature of the SF-GPR signals and the fact that the ground surface in general is rough and not perfectly flat, near surface buried mines are difficult to detect. To reduce these problems we suggest a clutter reduction approach based on subspace decomposing using PCA[7].

To employ the PCA subspace decomposition on the SF-GPR signals a vector space must be defined. The space observed is spanned by the multi-channel SF-GPR time-signal given by the signal matrix $\boldsymbol{S} \in \mathbb{R}^{M \times N}$ expressed by

$$\boldsymbol{S} = \{S_{m,n}\} = \{\boldsymbol{s}_m(n)\} = [\boldsymbol{s}(1), \boldsymbol{s}(2), \cdots, \boldsymbol{s}(N)], \tag{1}$$

where M is the number of one-dimensional scans considered and N is the number of samples in each of the considered one-dimensional scan in the signal matrix $\boldsymbol{S}$, and $\bar{s}_m(n)$ is given by the mean value

$$\bar{s}_m(n) = \bar{s}_{ij}(n) = s_{ij}(n) - \frac{1}{IJ}\sum_{i=1}^{I}\sum_{j=1}^{J} s_{ij}(n), \quad m = i + (j-1)I, \quad i \in [1; I], \quad j \in [1; J], \quad m \in [i; JI], \tag{2}$$

where $s_{i,j}(n)$ denotes the SF-GPR time-signal[†] one-dimensional scan received at the antenna located at $(x, y) = \big(x = (i-1)\triangle x, y = (j-1)\triangle y\big)$, where $i = 1, 2, \cdots, I$, and $j = 1, 2, \cdots, J$. $\triangle x$ and $\triangle y$ are the antenna location step size in the x- and y-direction, respectively. That is, in the signal matrix $\boldsymbol{S}$, i.e., $\bar{s}_m(n)$, $n = 1, 2, \cdots, N$ is the m'th signal, or in practice, the m'th one-dimensional scan in the time-domain subtracted by the mean value of the ensemble of considered one-dimensional scans.

The PCA subspace decomposition of the time-signals in $\boldsymbol{S}$ is based on a linear transformation, which produces uncorrelated sequences having decreasing variance of information for time-series in $\boldsymbol{S}$. In practice, it is the SVD that is used to perform the PCA subspace decomposition. For a given choice of $P \leq M$, the SVD of $\boldsymbol{S}$ can be expressed as[5]

$$\boldsymbol{X} = \boldsymbol{U}\boldsymbol{D}\boldsymbol{V}^{\mathrm{T}} = \sum_{i=1}^{P} \boldsymbol{u}_i D_{i,i} \boldsymbol{v}_i^{\mathrm{T}}, \quad P = \min\{M, N\}, \tag{3}$$

where the $M \times N$ matrix $\boldsymbol{U} = \{U_{m,i}\} = [\boldsymbol{u}_1, \boldsymbol{u}_2, \cdots, \boldsymbol{u}_N]$ and $N \times N$ matrix $\boldsymbol{V} = \{V_{n,i}\} = [\boldsymbol{v}_1, \boldsymbol{v}_2, \cdots, \boldsymbol{v}_N]$ represents the orthogonal basis vectors, i.e., eigenvectors of the symmetric matrices $\boldsymbol{S}\boldsymbol{S}^T$ and $\boldsymbol{S}^T\boldsymbol{S}$, respectively. $\boldsymbol{D}$ is an $N \times N$ diagonal matrix of singular values ranked in decreasing order, as expressed by $D_{i-1,i-1} \geq D_{i,i}, \forall i \in [2; N]$. The SVD identifies a set of uncorrelated time sequences given by the PC's: $\boldsymbol{y}_i = D_{i,i}\boldsymbol{v}_i$, enumerated by the component index $i = 1, 2, \ldots, N$. That is, we can write the observed signal matrix as a weighted sum of fixed eigenvectors,

[†]The Fourier transform given by $s_{ij}(n) \leftrightarrow \Gamma_{ij}(\omega)$

$\boldsymbol{u}_i$. The i'th PC constitutes the normalized linear combinations of samples in the signal matrix $\boldsymbol{S}$ with maximum variance under the constraint that it is orthogonal to all the other PC's, i.e., $\boldsymbol{y}_i^T \boldsymbol{y}_k = 0, \forall k \neq i$.

It is possible to remove uninteresting subspaces in $\boldsymbol{S}$, e.g., the air-to-ground reflection, by projection onto an M-dimensional subspace spanned by a number of PC's, as shown by,

$$\boldsymbol{Y} = \tilde{\boldsymbol{U}}^T \boldsymbol{S}, \quad \tilde{\boldsymbol{U}} = [\boldsymbol{u}_{i1}, \boldsymbol{u}_{i2}, \cdots, \boldsymbol{u}_{iM}],\ i_j \in [1; N],\ j = 1, 2, \cdots, M \tag{4}$$

where $\boldsymbol{Y}$ is an $M \times N$ matrix, i.e., $\boldsymbol{Y} = [\boldsymbol{y}_1, \boldsymbol{y}_2, \cdots, \boldsymbol{y}_M]^{\mathrm{T}}$. By identifying time peak locations of the power of the PC signals, y_i that correspond to the air-to-ground reflection and exclude such components, the air-to-ground reflection is suppressed. The scans are reconstructed as

$$\hat{\boldsymbol{S}} = \tilde{\boldsymbol{U}} \boldsymbol{Y}. \tag{5}$$

Examples and results of this approach are shown in Section 5.

3. FOCUSING OF THE SF-GPR SIGNALS: A SF-SAR APPROACH

Imaging techniques can be deployed on the SF-GPR signals to focus the reflected signals from the targets and thereby increase the signal-to-noise ratio. The approach considered in this paper is inspired by optical signal processing of an input in the front focal plane of a plano-convex lens[8].

Consider a monostatic SF-GPR that collects the data in the xy-plane at $z = 0$. The collected data is described by the reflection coefficient[6] $\Gamma(x, y, \omega)\big|_{z=0}$. Since the collected frequency data can be approximated by the diffracted field from an aperture illuminated by a plane wave and then using Huygen's Principle[8], we can express the collected field by

$$\Gamma(x, y, \omega)\big|_{z=0} = \frac{1}{j\lambda} \int_{-\infty}^{\infty} \int_{-\infty}^{\infty} \int_{-\infty}^{\infty} g(x_t, y_t, z_t) \frac{e^{j\boldsymbol{k}\cdot\boldsymbol{r}}}{|\boldsymbol{r}|} dx_t dy_t dz_t, \tag{6}$$

where $g(x_t, y_t, z_t)$ is a given source distribution in the ground, $\boldsymbol{k}$ is the wavenumber vector given by $\boldsymbol{k} = k_x \hat{x} + k_y \hat{y} + k_z \hat{z}$, $\boldsymbol{r}$ is the position vector given by $\boldsymbol{r} = (x - x_t)\hat{x} + (y - y_t)\hat{y} + (z - z_t)\hat{z}$, and λ is the wavelength.

The objective of the focusing procedure is to reconstruct the source distribution given by $g(x_t, y_t, z_t)$, which describes the reflecting surfaces of the targets. The focusing can be obtained through the optical signal processing, by using the signal processing properties of the plano-convex lens[8] and Huygen's Principle.

From the optical signal processing given by the signal processing describing the plano-convex lens we can, if we assume homogeneous ground and flat ground surface, reconstruct the reflection surface from the 3-D Fourier transform given by

$$g(x, y, z)\Big|_{t=0} = \int_{-\infty}^{\infty} \int_{-\infty}^{\infty} \int_{-\infty}^{\infty} G(k_x, k_y, \omega) e^{j\sqrt{(k^2 - k_x^2 - k_y^2)} \cdot z} e^{-jk_x x} e^{-jk_y y} e^{j\omega t} dk_x dk_y d\omega \Big|_{t=0} \tag{7}$$

where

$$G(k_x, k_y, \omega) = \int_{-\infty}^{\infty} \int_{-\infty}^{\infty} \Gamma(x, y, \omega)\big|_{z=0} e^{jk_x x} e^{jk_y y} dx dy \tag{8}$$

By stepping with small steps in the z-direction an image can be constructed using (7). Focusing the SF-GPR data in this way provides that the propagation velocity kan be changed. In the results, shown in Section 5, the SF-GPR data is focused in two dimensions only, i.e., $k_y = 0$. This approach can largely be carried out in the frequency domain by using FFT's.

4. SIMULATED SF-GPR SIGNALS

The clutter reduction and resolution enhancement approaches presented in this paper are evaluated on simulated data. The data includes an M56 dummy non-metallic mines and an M56 shaped iron mines buried in sand. The simulated data are obtained by simulating a field-test setup using the finite-difference time-domain (FD-TD) numerical method[12].

The SF-GPR Data

Figure 1 shows the coordinates in a (x,y,z) cartesian coordinate system used for each simulation setup. The used mines are a metallic M-56 shaped AP landmine and a non-metallic M-56 dummy AP landmine. All the objects have the same irregular shape with a diameter of 5.4 cm and a height of 4.0 cm.

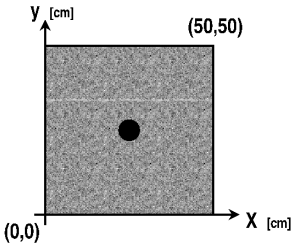

Object	M-56 dummy	iron
x-position (cm)	25	25
y-position (cm)	25	25
z-position, depth from the surface (cm)	5	5
Permeability, μ_r	1	2000
Permittivity, ε_r	2.6	1
Conductivity, σ (S/m)	0.03	$1.03 \cdot 10^7$

Figure 1. The mines considered in this study is a non-metallic M56 dummy mine filled with beeswax and an M56 shaped mine made of iron. The black mark in the coordinate system indicates a mine and the corner-coordinates indicate the number of measurement points in the x- and x-direction, respectively. Each measurement point were located 1 cm × 1 cm from each other. The table to the right gives the position and dielectric and magnetic properties of the objects.

In our simulations, the interface between the ground and the air is modeled rough surface. The surface roughness is assumed to have a Gaussian spectrum[9]. The spatial correlation function for the rough surface as a function of position x is expressed as

$$p(x) = h^2 e^{-x^2/l}, \tag{9}$$

where h is the rms surface height and l the correlation length. The surface profile varies randomly between surfaces of different rms roughness. In the simulations the following rms-roughness and correlation length values were used: $h_1 = 0.5cm$, $h_2 = 1.0cm$, $h_3 = 2.0cm$, $l_1 = 0.5cm$, $l_2 = 1.0cm$, and $l_3 = 2.0cm$.

SF-GPR Data Simulation

By convenience we confine to a two-dimensional SF-GPR data simulatation (x, z) using the FD-TD method[12] and impose a rotational symmetry, although a full 3D simulation is feasible. The method incorporates a lossy half space, a rough surface, buried dielectric objects and good conducting objects. The simulations are using transverse electric magnetic (TEM) fields. For a 2-D medium, the TEM field from a line source can be expressed as[11]

$$\boldsymbol{E} = \hat{y} E_0 e^{j(\omega t + \boldsymbol{k}\cdot\boldsymbol{r})}. \tag{10}$$

The wave propagation through the medium (air, ground, and targets) can be expressed by the wave equation given by[1]

$$\frac{\partial^2 \boldsymbol{E}}{\partial x^2} + \frac{\partial^2 \boldsymbol{E}}{\partial z^2} = \mu\varepsilon \frac{\partial^2 \boldsymbol{E}}{\partial t^2} + \mu\sigma \frac{\partial \boldsymbol{E}}{\partial t}, \tag{11}$$

where $\mu = \mu_0 \mu_r$ is the absolut permeability, $\mu_0 = 1.26 \times 10^{-6}$H/m is the absolute magnetic permeability of free space, μ_r is the relative magnetic permeability, $\varepsilon = \varepsilon_0 \varepsilon_r$ is the absolute electric permittivity, $\varepsilon_0 = 8.8542 \times 10^{-12}$F/m, and ε_r is the relative permittivity.

Using (10) and (11) and absorbing boundary conditions given by Engquist-Majda,[12] the FD-TD simulations were done.

5. EXAMPLE RESULTS ON CLUTTER REDUCTION COMBINED WITH RESOLUTION ENHANCEMENT

The imaging approach for resolution enhancement, the PCA approach, and the classical mean-subtraction method for clutter reduction were deployed on the simulated data for evaluating the proper clutter reduction combined with resolution enhancement. The results of our approaches are best illustrated by the following examples, which are the simulated examples described in Section 4.

The results are shown in Figure 2 to 11. Figure 2 to 5 shows examples of the choice of PC's in the PCA based reconstruction method, and Figure 6 to 11 shows results of the clutter reduction combined with resolution enhancement. The results are visualized using two-dimensional scans across the mine.

The PCA based Reconstruction

The PCA method were deployed on the signal matrix $\boldsymbol{S}$ as described in Section 2. Each eigenimage summarizes the reflection associated with the time signature given by the corresponding PC time signal. Figures 2 to 5 shows examples of the power of the PC signals and associate eigenimages. The power is calculated using a non-causal Kaiser window of size 3 with a characteristic parameter of 2π. If the PC time is rather peaked, then the eigenimage corresponds to the reflection from the depth related to that peak location. Furthermore, the variance of the PC's decreases with the PC number, indicating the strength of the reflections from various depth. Figure 6 to 11 shows comparison between the previous mentioned mean-subtraction method and the PCA based reconstruction of the signal matrix. The third row in the figures are the example results from the PCA based reconstruction method. From the results it is clear that the mine signal is more pronounced, and the suppression of the ground reflection seems satisfactory. However, when the ground surface roughness gets to high it also seems that the PCA method fails. But for small fluctuations in the ground surface the PCA works satisfactory.

The Mean-Subtraction Clutter Reduction

The PCA based reconstruction approach is compared to the classic mean-subtraction method. Results on mean-subtraction is given in the second row in the Figures 6 to 11. From the results it is clear that the mean-subtraction method fails. Even at a small rms-roughness (0.5 cm) there still exist a lot of surface reflection in the signal. As expected the M56 dummy mine (non-metallic) is much harder to detect than the iron M56 mine-like target, since the reflections are very small.

The Focusing of the SF-GPR signals

In the right panel of Figure 6 to 11 the focused SF-GPR data of the results are given in the left panel of Figure 6 to 11. From the results it is clear that the focused mine reflection is more pronounced when proper clutter reduction has been deployed on the SF-GPR data.

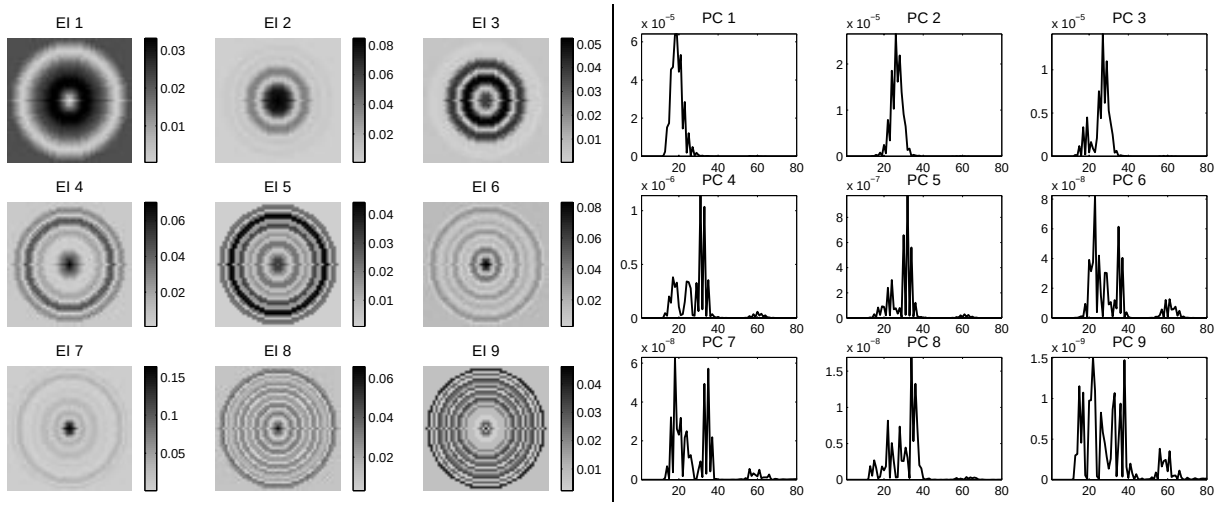

Figure 2. *Iron M56 Mine-like Target, Example 1*: The left panel shows the eigenimages (in xy-plane) and the right panel shows the associated principal components (PC's), for the simulated example with rms-roughness of 0.5 cm and correlation length of 50 cm. From the PC's it is clear that PC1 shows a peak close to the ground surface (the ground surface is located near sample 20 and the iron M56 mine-like target is located near sample 25), and the associate eigenimage provides the fluctuations in the ground surface. PC2 peaks much later and the associate eigenimage clearly has a strong mine signature. Subsequent PC's becomes less focused in time and the eigenimages show a clutter like texture. Also notice that the power of the PC's decrease with the number, indicating that the surface reflection has the strongest power, the mine signal has a smaller power, and clutter has lowest power. Much of the ground reflection can be removed by removing PC1.

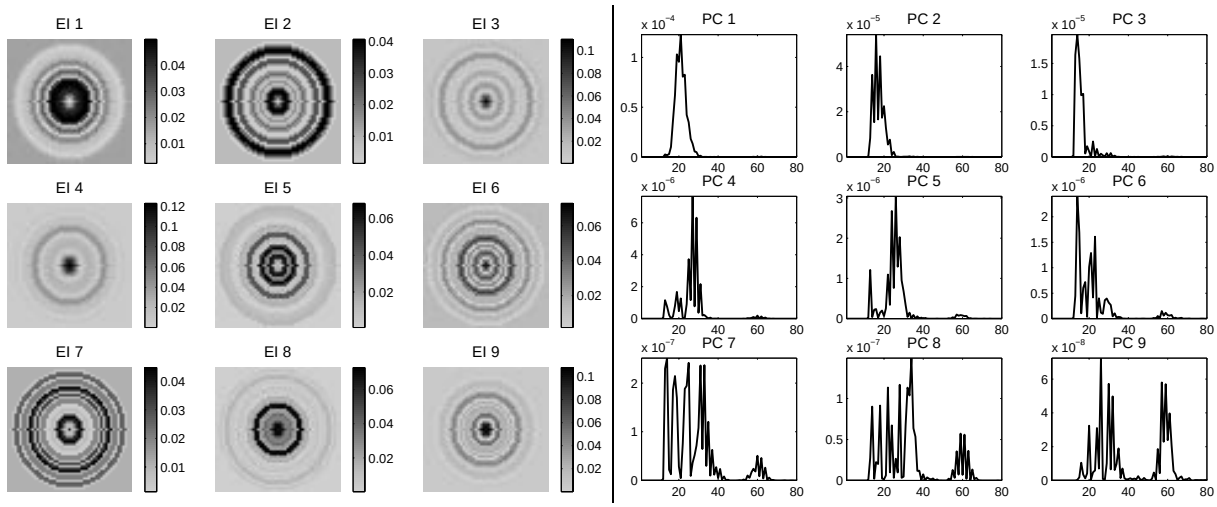

Figure 3. *Iron M56 Mine-like Target, Example 2*: The left panel shows the eigenimages (in xy-plane) and the right panel shows the associated principal components (PC's), for the simulated example with rms-roughness of 2 cm and correlation length of 10 cm. From the PC's it is clear that PC1, PC2, and PC3 shows a peak close to the ground surface (the ground surface is located near sample 20 and the iron M56 mine-like target is located near sample 25), and the associate eigenimage provides the fluctuations in the ground surface. PC4 peaks much later and the associate eigenimage clearly has a strong mine signature. In this example we can remove much of the ground reflection by removing PC1, PC2 and PC3.

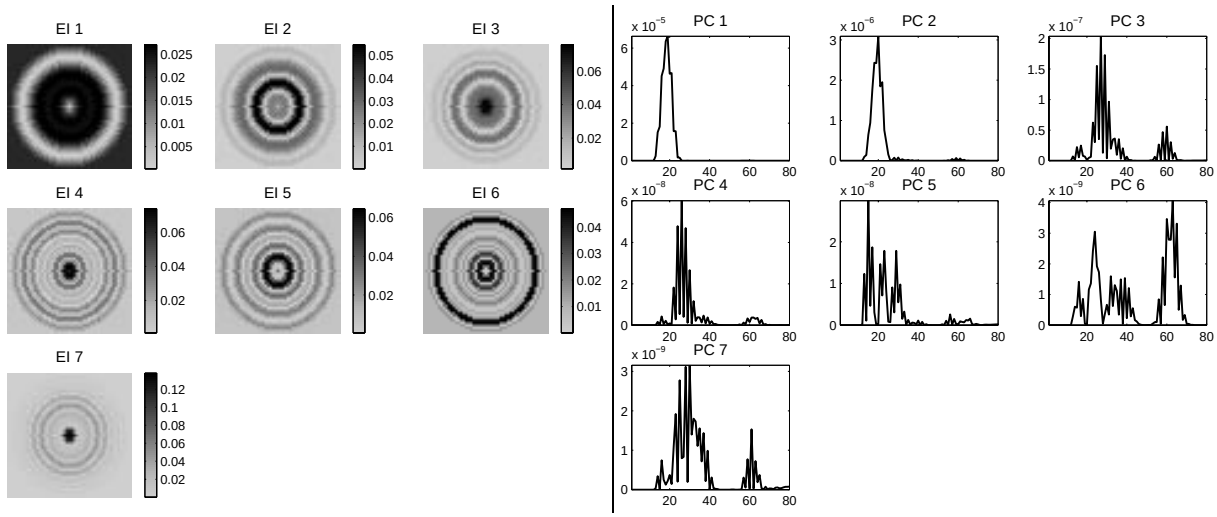

Figure 4. *M56 Dummy Mine, Example 1*: The left panel shows the eigenimages (in xy-plane) and the right panel shows the associated principal components (PC's), for the simulated example with rms-roughness of 0.5 cm and correlation length of 50 cm. Similar to the two previous examples by removing PC1 and PC2 much of the ground reflection can be removed.

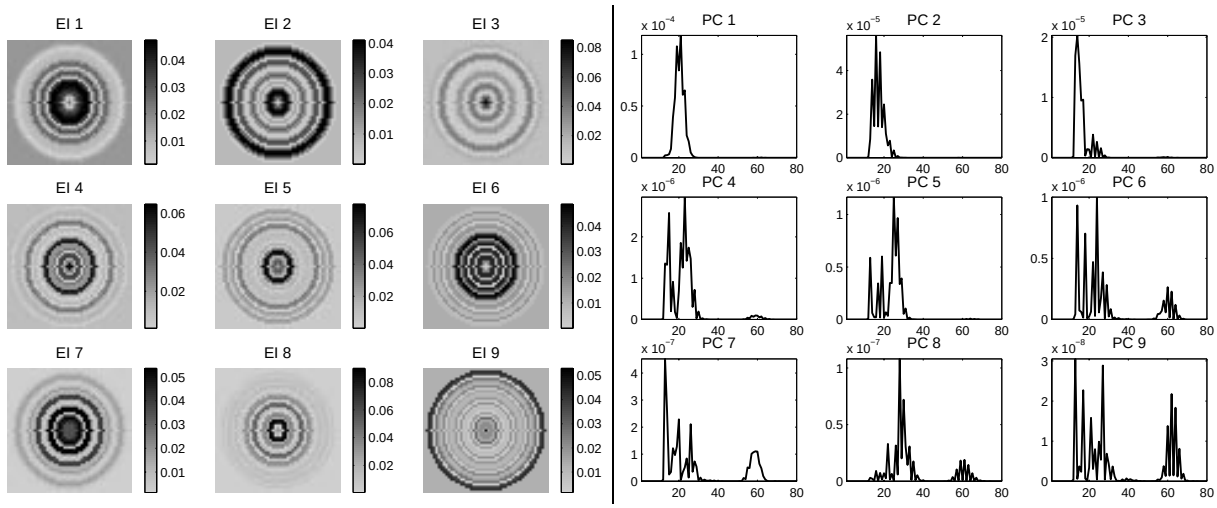

Figure 5. *M56 Dummy Mine, Example 2*: The left panel shows the eigenimages (in xy-plane) and the right panel shows the associated principal components (PC's), for the simulated example with rms-roughness of 2 cm and correlation length of 10 cm. Again, removing PC1, PC2 and PC3 will reduce the ground reflection. Notice that the more the surface fluctuates the higher is the number of PC's that must be removed.

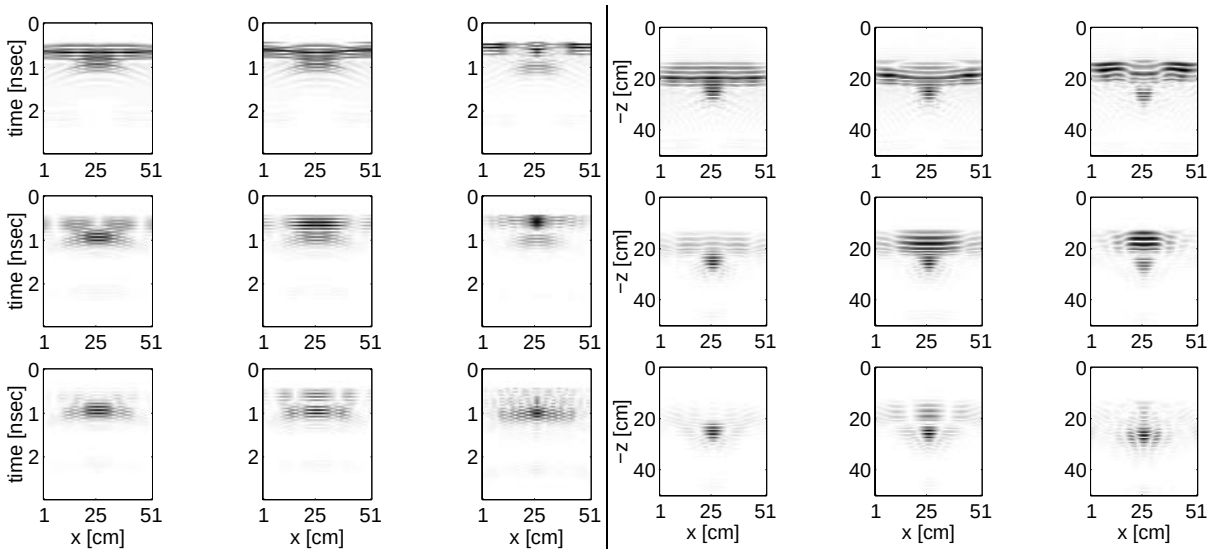

Figure 6. *Iron M56 Mine-like Target*: The images shows two-dimensional scans across the mine for a correlation length of 50 cm. Left panel: From left to right and top to down we have 1) rms = 0.5 cm, raw SF-GPR data 2) rms = 1.0 cm, raw SF-GPR data 3) rms = 2.0 cm, raw SF-GPR data 4) rms = 0.5 cm, mean-subtracted 5) rms = 1.0 cm, mean-subtracted 6) rms = 2.0 cm, mean-subtracted 7) rms = 0.5 cm, PCA reconstructed 8) rms = 1.0 cm, PCA reconstructed 9) rms = 2.0 cm, PCA reconstructed. Right panel: The focused two-dimensional scans from left panel.

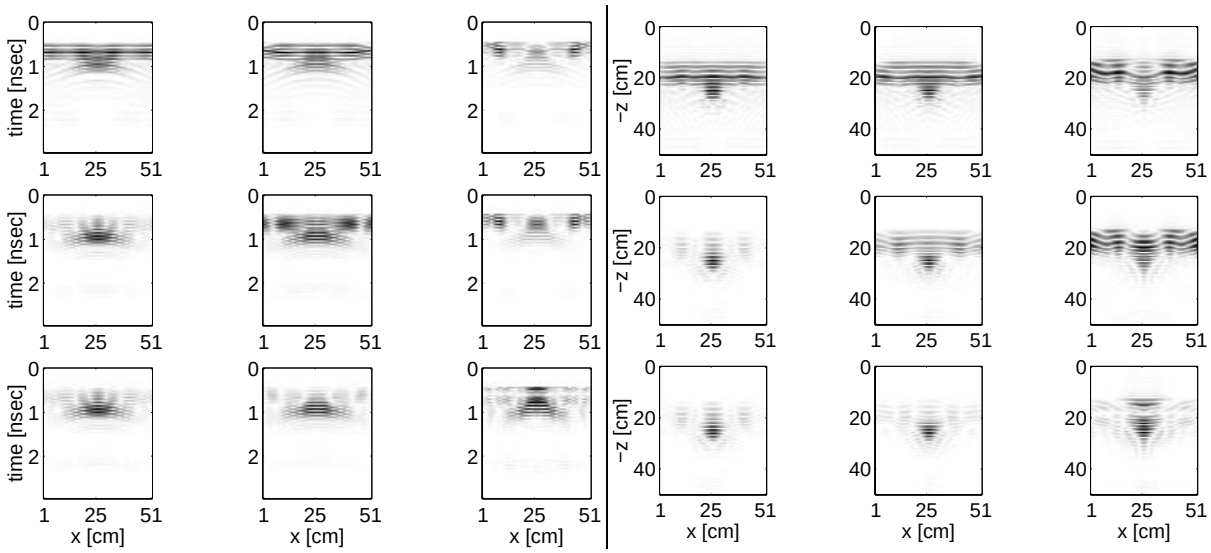

Figure 7. *Iron M56 Mine-like Target*: The images shows two-dimensional scans across the mine for a correlation length of 30 cm. Left panel: From left to right and top to down we have 1) rms = 0.5 cm, raw SF-GPR data 2) rms = 1.0 cm, raw SF-GPR data 3) rms = 2.0 cm, raw SF-GPR data 4) rms = 0.5 cm, mean-subtracted 5) rms = 1.0 cm, mean-subtracted 6) rms = 2.0 cm, mean-subtracted 7) rms = 0.5 cm, PCA reconstructed 8) rms = 1.0 cm, PCA reconstructed 9) rms = 2.0 cm, PCA reconstructed. Right panel: The focused two-dimensional scans from left panel.

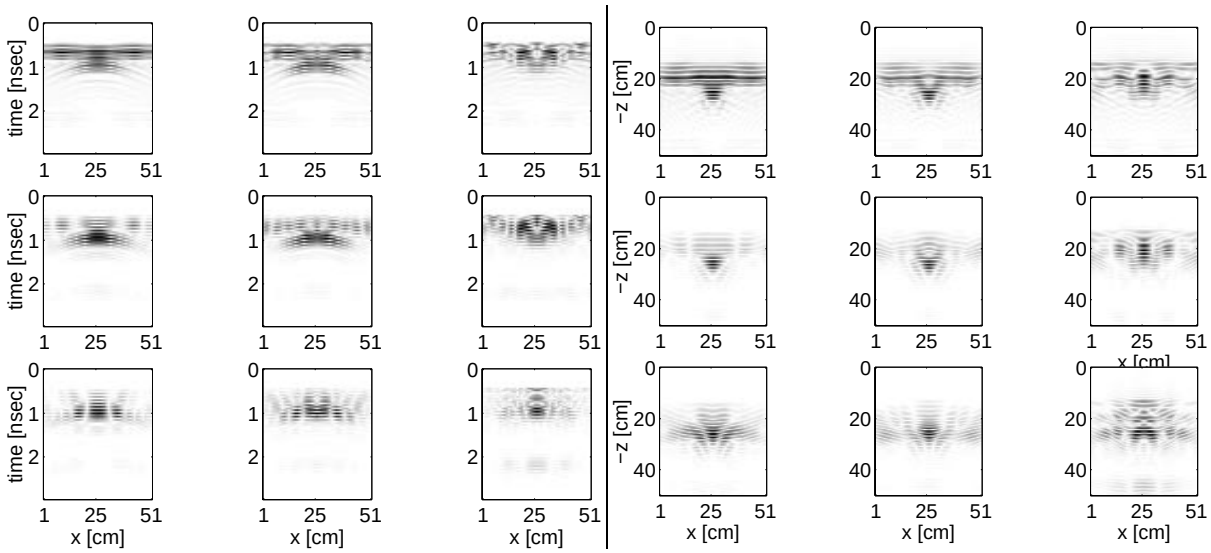

Figure 8. *Iron M56 Mine-like Target*: The images shows two-dimensional scans across the mine for a correlation length of 10 cm. Left panel: From left to right and top to down we have 1) rms = 0.5 cm, raw SF-GPR data 2) rms = 1.0 cm, raw SF-GPR data 3) rms = 2.0 cm, raw SF-GPR data 4) rms = 0.5 cm, mean-subtracted 5) rms = 1.0 cm, mean-subtracted 6) rms = 2.0 cm, mean-subtracted 7) rms = 0.5 cm, PCA reconstructed 8) rms = 1.0 cm, PCA reconstructed 9) rms = 2.0 cm, PCA reconstructed. Right panel: The focused two-dimensional scans from left panel.

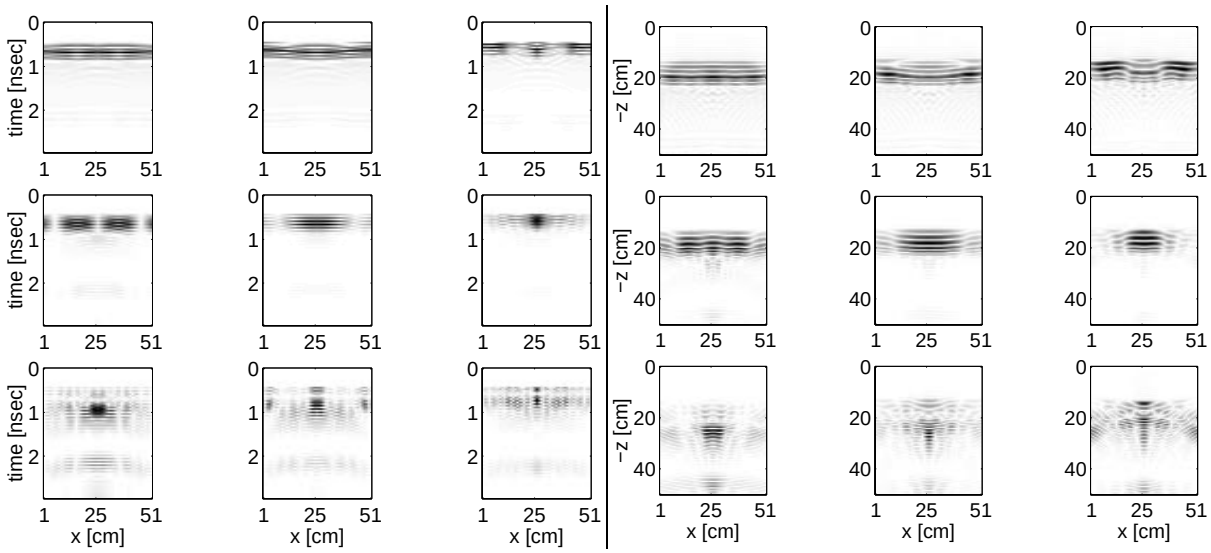

Figure 9. *M56 Dummy mine*: The images shows two-dimensional scans across the mine for a correlation length of 50 cm. Left panel: From left to right and top to down we have 1) rms = 0.5 cm, raw SF-GPR data 2) rms = 1.0 cm, raw SF-GPR data 3) rms = 2.0 cm, raw SF-GPR data 4) rms = 0.5 cm, mean-subtracted 5) rms = 1.0 cm, mean-subtracted 6) rms = 2.0 cm, mean-subtracted 7) rms = 0.5 cm, PCA reconstructed 8) rms = 1.0 cm, PCA reconstructed 9) rms = 2.0 cm, PCA reconstructed. Right panel: The focused two-dimensional scans from left panel.

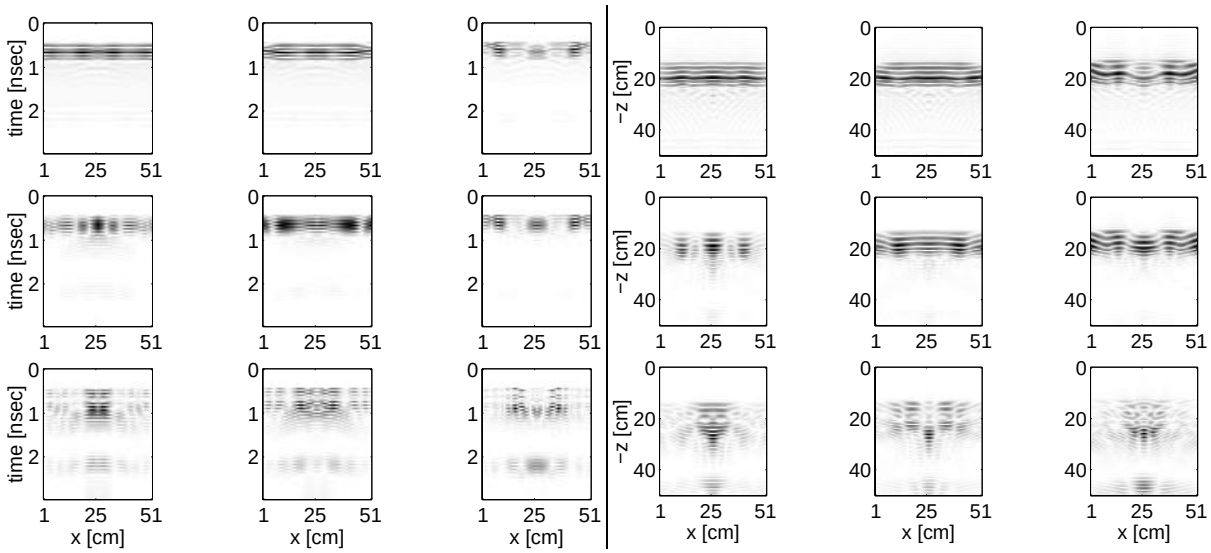

Figure 10. *M56 Dummy mine*: The images shows two-dimensional scans across the mine for a correlation length of 30 cm. Left panel: From left to right and top to down we have 1) rms = 0.5 cm, raw SF-GPR data 2) rms = 1.0 cm, raw SF-GPR data 3) rms = 2.0 cm, raw SF-GPR data 4) rms = 0.5 cm, mean-subtracted 5) rms = 1.0 cm, mean-subtracted 6) rms = 2.0 cm, mean-subtracted 7) rms = 0.5 cm, PCA reconstructed 8) rms = 1.0 cm, PCA reconstructed 9) rms = 2.0 cm, PCA reconstructed. Right panel: The focused two-dimensional scans from left panel.

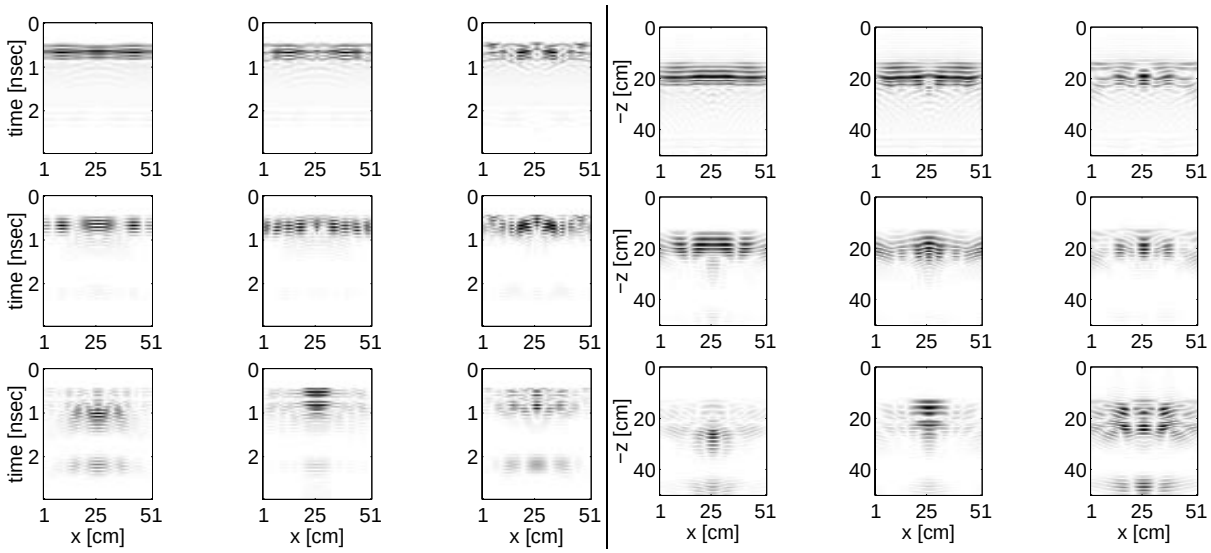

Figure 11. *M56 Dummy mine*: The images shows two-dimensional scans across the mine for a correlation length of 10 cm. Left panel: From left to right and top to down we have 1) rms = 0.5 cm, raw SF-GPR data 2) rms = 1.0 cm, raw SF-GPR data 3) rms = 2.0 cm, raw SF-GPR data 4) rms = 0.5 cm, mean-subtracted 5) rms = 1.0 cm, mean-subtracted 6) rms = 2.0 cm, mean-subtracted 7) rms = 0.5 cm, PCA reconstructed 8) rms = 1.0 cm, PCA reconstructed 9) rms = 2.0 cm, PCA reconstructed. Right panel: The focused two-dimensional scans from left panel.

6. CONCLUSION

This paper presents a combined clutter reduction and resolution enhancement approach based on PCA and knowledge from optical signal processing. In order to evaluate the clutter reduction combined with resolution enhancement in SF-GPR data, data are simulated using the Finite-Difference Time-Domain numerical method. In general, the simulated data are two-dimensional, but by assuming that the antenna is rotational symmetric the three-dimensional data are constructed by rotating the two-dimensional data. From the results it is clear that proper clutter reduction before focusing is valuable. The resolution enhancement method gives satisfactory results. From the focused SF-GPR data it is clear that the data are indeed focused. However, the method only concerns focusing using the time-dependence $e^{j\omega t}$. The results may be improved by also including the losses in the ground. The PCA based reconstruction method gives satisfactory results only, when we use the knowledge about the depth in which the mine is located which is not a priori knowledge in mine clearance. The air-to-ground reflection and clutter are mainly represented in few principal components. Omitting these components in the subsequent reconstruction of the signals enables promising suppression of the air-to-ground reflection and the clutter. However, some of the valuable information in the mine signals may be lost, which is unsatisfactory. Future studies will involve automatic selection of the principal components to be retrained, as well as related techniques, e.g., independent components analysis[5] (ICA). Our belief is that ICA would produce more peaked components, providing for a better separation between the air-to-ground reflections, the reflections from the mines, and from the clutter. In addition we plan to use the PCA based features as the input to a nonlinear statistical supervised detection algorithm. One feature that may be used advantageously is that the PCA identifies reflection surfaces that are symmetric.

7. ACKNOWLEDGEMENTS

The authors would like to thank Staffan Abrahamson, Dan Axelson, Anders Friedmann and Anders Gustafson from the Division of Sensor Technology, National Defense Research Establishment (FOA), Linköping, Sweden, for their support during data collections at FOA. Ole Nymann is acknowledged for stimulating discussions.

REFERENCES

1. H.W. Chen & T.M. Huang: "Finite-difference time-domain simulation of GPR data", *Journal of Applied Geophysics 40*, pp. 139–163, 1998.
2. D.J. Daniels: *Surface Ground Penetrating Radar*, London: IEE, 1996.
3. E. Fisher & G.A. Mcmechan: "Examples fro reverse-time migration of single-channel ground penetrating radar profiles", *Geophysics*, vol. 57, no. 4, pp. 577–586, 1992.
4. A. Gynatilaka & B.A. Beartlein: "A subspace decomposition technique to improve GPR imaging of anti-personnel mines",*Detection and Remediation Technologies for Mines and Minelike Targets V*,Proceedings of SPIE, vol. 4039, pp. 1008–1018, 2000.
5. L.K. Hansen, J. Larsen & T. Kolenda: "On Independet Componenet Analysis for Multimedia Signals", in L. Guan, S.Y. Kung & J. Larsen (eds.) *Multimedia Image and Video Processing*, CRC Press, Ch. 7, pp. 175–199, 2000.
6. K.B. Jakobsen, H.B.D. Sørensen & O. Nymann: "Stepped-Frequency Ground- Penetrating-Radar for Detection of Small Non-metallic Buried Objects", *Detection and Remediation Technologies for Mines and Minelike Targets II*, vol. 3079, pp. 538–542, 1997.
7. B. Karlsen, J. Larsen, K.B. Jakobsen, H.B.D. Sørensen: "Antenna Characteristics and Air-Ground Interface Deembedding Methods for Stepped-Frequency Ground Penetrating Radar Measurements", *Detection and Remediation Technologies for Mines and Minelike Targets V*, vol. 4039, pp. 1420–1430, 2000.
8. K. Lizuka: *Engineering Optics*, Berlin Heidelberg: Springer-Verlag, 2nd edition, 1987.
9. A.v.d Merwe, I.J. Gupta & L. Peters: "A Clutter Reduction Technique for GPR Data from Mine Like Targets", *Detection and Remediation Technologies for Mines and Minelike Targets IV*, vol. 3710, pp. 1094–1101, 1999.
10. R.H. Stolt: "Migration by Fourier Transform",: *Geophysics*, vol. 43,no. 1, pp. 23–48, 1978.
11. D.M. Pozar: *Microwave Enginering*, 2.nd ed., Singapore: Mcgraw-Hill Inc., 1980.
12. A. Taflove: *Computational Electrodynamics: the finite-difference time- domain method*, Artech House Inc., 1995.
13. S.H. Yu & T.R. Witten: "Automatic Mine Detection based on Ground Penetrating Radar", *Detection and Remediation Technologies for Mines and Minelike Targets IV*, vol. 3710, pp. 961–972, 1999.